Nonlinear Stiffness and Vibration Frequency Analyses of the Conventional Spring-suspended Segment Model

Changqing Wu, Shun Wang, Hua Luo, Guanghui Wang

***Abstract*—Wind tunnel tests using spring-suspended segment models (SSMs) are extensively used to examine the wind-resistance performance of long-span bridges. Conventional SSMs typically assume constant stiffness regardless of vibration amplitudes; however, this holds only for low amplitudes. At higher amplitudes, stiffness exhibits a nonlinear behaviour. This study presents a theoretical investigation of the stiffness nonlinearity in conventional SSMs. A 2D mechanical model is developed with appropriate simplifications to derive amplitude-dependent equivalent vertical and torsional stiffnesses expressions. Using given SSM parameters, equivalent stiffness and frequency values are computed for torsional amplitudes ranging from 0° to 20° and vertical amplitudes from 0 to 0.20 m. The results reveal significant amplitude-dependent nonlinearity in torsional stiffness and frequency; at 20° torsional amplitude, equivalent torsional stiffness decreases by 24.64%, and torsional frequency decreases by 13.19%. To limit geometric nonlinearity, a torsional amplitude < 5° is recommended. Vertical vibrations have negligible effects on torsional stiffness; at 20° torsional amplitude, a 0.20 m vertical amplitude reduces the torsional stiffness by only 2.73%. Neither vertical nor torsional vibrations affect the equivalent vertical stiffness. These findings highlight the need for incorporating nonlinear torsional stiffness and frequency in analyses to improve accuracy when using conventional SSMs for aerodynamic derivative identification and wind-resistance performance evaluations under large-amplitude vibration conditions.**

***Index Terms*—bridge segment model, spring-suspended segment model, stiffness nonlinearity, theoretical study**

I. INTRODUCTION

SPRING-suspended segment models (SSMs) have been widely adopted in wind tunnel tests to examine aerodynamic derivatives and wind-induced vibration characteristics of bridge decks [1]–[5]. As a critical mechanical parameter, the stiffness of an SSM is typically determined through its free-decay vibration response. Conventionally, the stiffness of an SSM is typically assumed to be constant, which is acceptable for studies on the flutter critical wind speed and the characteristics of small-amplitude vortex-induced vibration (VIV) [6]–[9]. However, when examining large-amplitude nonlinear post-flutter and VIV, vertically extended springs experience significant inclination, leading to nonlinear variations in the geometric stiffness, with the torsional stiffness provided by the springs exhibiting particularly pronounced amplitude-dependent nonlinear behaviour.

Neglecting the nonlinear stiffness characteristics of SSMs in studies on the nonlinear post-flutter and large-amplitude VIV in bridges can introduce errors in experimental results, compromising the accurate evaluation of wind-resistant performance. VIV is a resonance phenomenon triggered when the vortex shedding frequency approaches the structural natural frequency within specific wind speed ranges and may exhibit deviations in the predicted lock-in wind speed intervals due to stiffness nonlinearities altering the natural frequencies, leading to potential discrepancies between the predicted and actual VIV wind speed ranges. Furthermore, existing research on nonlinear flutter has predominantly employed SSMs in wind tunnel tests, and the results have revealed that post-flutter limit cycle oscillations (LCOs) arise from structural or aerodynamic nonlinearities [10]–[13]. These findings collectively indicate that stiffness nonlinearities of conventional SSMs significantly influence the identification of nonlinear parameters and prediction accuracy of nonlinear flutter responses in bridge engineering applications.

Recent wind tunnel tests have demonstrated that conventional SSMs exhibit significant nonlinear mechanical behaviour under large-amplitude vibrations, irrespective of the presence of wind [14]–[17]. Free-decay vibration tests conducted under wind-free conditions have revealed amplitude-dependent nonlinearities in the stiffness and vibration frequency of conventional SSMs, showing progressive reductions with increasing amplitudes [17]–[22]. This nonlinearity stems from both fluid–structure interaction-induced added mass effects [23]–[25] and geometric nonlinearities in springs under large displacements. However, existing studies have not systematically isolated the relative contributions of these mechanisms. To address this issue, Xu et al. [26] investigated the geometric nonlinear stiffness of the conventional SSM, deriving computational

Manuscript received April 19, 2025; revised August 17, 2025.

This work was supported in part by the Project Supported by the Department of Education of Hunan Province (Grant Nos. 23B0645 and 23A0496), and the Project Supported by the Regional Joint Fund of Hunan Provincial Natural Science Foundation (Grant Nos. 2025JJ70276 and 2024JJ7214).

Changqing Wu is a lecturer in College of Civil Engineering and Architecture, Hunan Institute of Science and Technology, Yueyang, 414000, China (e-mail: wuchangqing@hnist.edu.cn).

Shun Wang is a postgraduate student in College of Civil Engineering and Architecture, Hunan Institute of Science and Technology, Yueyang, 414000, China (e-mail: 822311140566@vip.hnist.edu.cn).

Hua Luo is an associate professor in College of Civil Engineering and Architecture, Hunan Institute of Science and Technology, Yueyang, 414000, China (e-mail: 12015024@hnist.edu.cn).

Guanghui Wang is an associate professor in College of Civil Engineering and Architecture, Hunan Institute of Science and Technology, Yueyang, 414000, China (e-mail: wgh325@hnist.edu.cn).

formulae for the vertical and torsional stiffnesses. Despite these efforts, the calculation formulae remain relatively complex, which may limit their practical implementation and wider application.

Building on previous studies, this study conducts a theoretical investigation into the nonlinear stiffness and vibration frequency of the conventional SSM, proposing analytical formulae to calculate its equivalent vertical and torsional stiffnesses. The effects of the vertical and torsional vibration amplitudes on the stiffnesses and frequencies of the SSM are quantitatively analysed, and the derived stiffness formulae are subsequently simplified based on this analysis.

The main contributions of this study are as follows: (1) establishment of a 2D mechanical model of the conventional SSM for equivalent stiffness calculations, with explicitly defined simplifications and assumptions; (2) derivation of amplitude-dependent analytical formulae for the equivalent vertical and torsional stiffnesses based on the proposed model; (3) computation of the equivalent vertical and torsional stiffness values based on given parameters and the proposed formulae, a quantitative assessment of the amplitude effects on the system stiffness and vibration frequencies, and formulation of simplified stiffness expressions based on these evaluations.

II. Nonlinear Stiffness of the Conventional SSM

A. 2D Model of the Conventional SSM

The conventional coupled bending–torsion two-degree-of-freedom (2-DOF) SSM mainly comprises eight tensioned springs and a rigid bridge segment model. At both ends of this model, rigid support arms suspend four upper and four lower springs, with four tightened horizontal wires symmetrically constraining the lateral motion in the model plane. To ensure symmetry, the upper and lower springs are vertically aligned, while the left–right and front–rear springs are symmetrically arranged about the torsional centre *O*.

For analytical simplification, the conventional SSM can be reduced to a 2D mechanical model, as illustrated in Fig. 1, where the segment model (denoted by *TK*) is suspended by four spring pairs (designated as *TA*, *TC*, *KB*, and *KD* respectively). Points *T* and *K* represent the spring-to-model connection points, with *r* denoting the lateral distance from the torsional centre of the sectional model to these connection points. The *x*-axis corresponds to the lateral direction, while the *y*-axis represents the vertical direction. Notably, each spring pair in the 2D model equivalently represents two co-lateral springs in the actual 3D suspension system.

To facilitate the derivation of the computational formulae for the equivalent nonlinear stiffnesses of the conventional SSM, this study applies the following assumptions:

(1) Four sufficiently long, tensioned horizontal wires connected to the torsional centre constrain the lateral displacements, whereby the segment model is assumed to perform exclusively torsional and vertical vibrations (2-DOF system), with lateral motion effects on the vertical and torsional stiffnesses being neglected.

(2) The centroid of the sectional model coincides with its torsional centre, thereby eliminating gravitational contributions to the torsional stiffness.

(3) Upper and lower springs are assumed to connect at identical points on rigid support arms, with dimensional characteristics of the support arms disregarded.

(4) Although actual suspension systems may exhibit either uniform or nonuniform stiffness among the four upper and four lower springs, for analytical convenience, all eight springs are postulated to maintain identical stiffness *k* with invariant properties. Moreover, the initial states (including pre-stress and undeformed lengths) are assumed identical within respective upper and lower spring groups.

(5) Co-lateral spring pairs (four groups) are postulated to exhibit synchronised vibrations during model motion, with all the eight springs remaining in tension throughout the dynamic responses.

(6) Within the range of the torsional amplitude studied in this work, the lateral force components of the spring elasticity are considered negligible compared with vertical counterparts, justifying the exclusion of their torque contributions about the torsional centre in subsequent theoretical derivations.

When the sectional model is at its equilibrium position, springs *TA* and *KB* have length *l* while springs *TC* and *KD* maintain length *n*. The initial force differential between the four spring pairs equilibrates the model weight *Mg*, satisfying:

$$4k(l-n)=Mg\ . \tag{1}$$

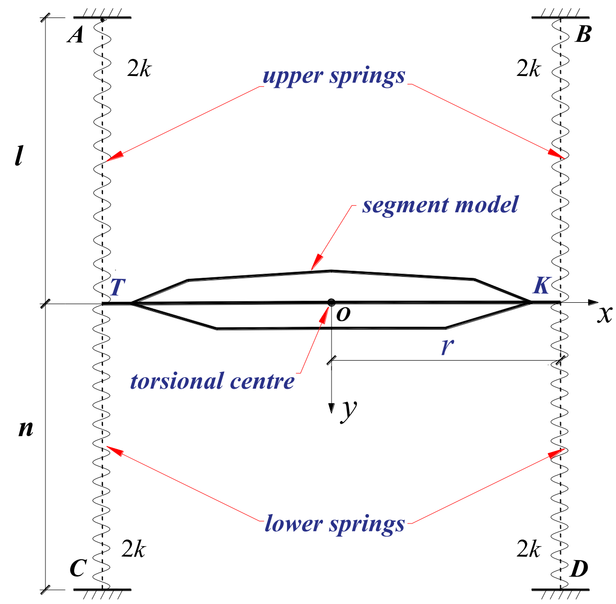

Fig. 1. 2D model diagram of the conventional SSM.

B. Mechanical Analysis Model and Equivalent Stiffness Formulae of the Conventional SSM

Under external excitation, the segment model undergoes coupled bending–torsion vibrations with a torsional amplitude α (defined as positive in the counter-clockwise direction) and a vertical amplitude *h* (positive downward). In this configuration, all the four spring pairs develop new restoring forces relative to their initial equilibrium states: F_{TA}, F_{TC}, F_{KB}, and F_{KD} denote the total restoring forces of springs *TA*, *TC*, *KB*, and *KD*, respectively; F_{TAy}, F_{TCy}, F_{KBy}, and F_{KDy} represent their vertical force components; while M_{TA}, M_{TC}, M_{KB}, and M_{KD} correspond to the moments generated by forces F_{TA}, F_{TC}, F_{KB}, and F_{KD} about the torsional centre, as shown in Fig. 2(a). After deformation, the geometric relationship diagram of the sectional model is shown in Fig. 2(b). β_1, β_2, β_3, and β_4 denote the angles between vectors $\overrightarrow{F_{TA}}$, $\overrightarrow{F_{TC}}$, $\overrightarrow{F_{KB}}$, $\overrightarrow{F_{KD}}$ and the horizontal direction, respectively; where θ_1, θ_2, θ_3, and θ_4 represent the angles between vectors $\overrightarrow{F_{TA}}$ and $\overrightarrow{TO}$, $\overrightarrow{F_{TC}}$ and $\overrightarrow{TO}$, $\overrightarrow{F_{KB}}$ and $\overrightarrow{KO}$, and $\overrightarrow{F_{KD}}$ and $\overrightarrow{KO}$, respectively.

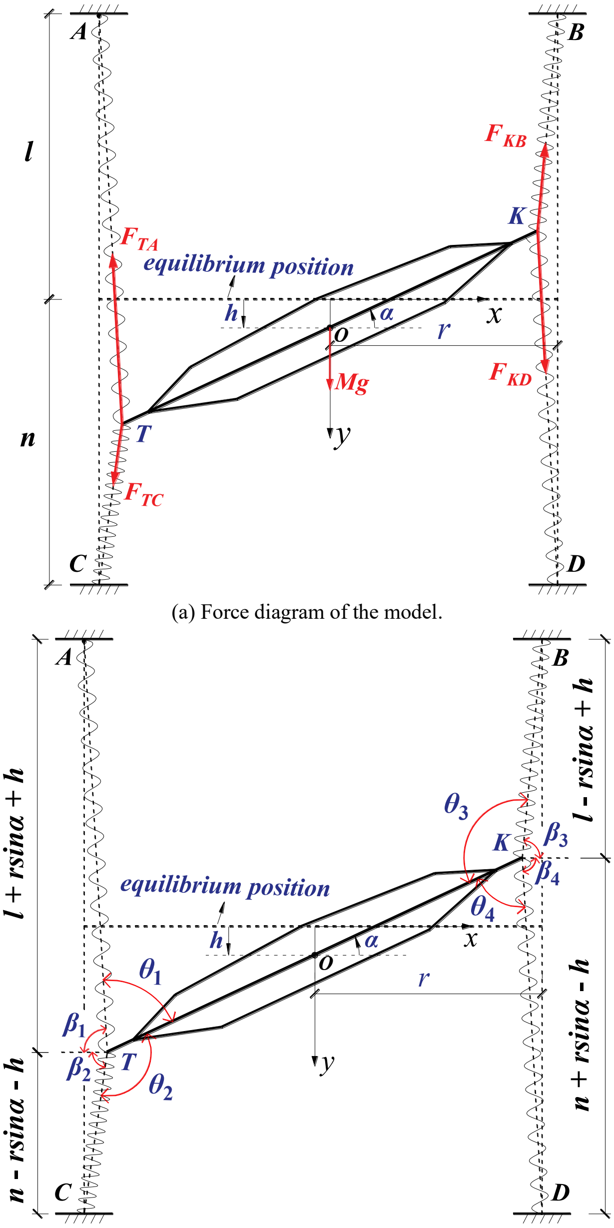

(a) Force diagram of the model.

(b) Geometric relationship diagram after deformation.

Fig. 2. 2D mechanical analysis model of the conventional SSM.

Taking spring TA as an example, its elastic force F_{TA} and moment M_{TA} about the torsional centre are derived based on Fig. 2. After deformation, the elongation of spring TA is:

$$\Delta l_{TA} = \sqrt{r^2(1-\cos\alpha)^2 + (l + r\sin\alpha + h)^2} - l \ . \tag{2}$$

The elastic force of spring TA can then be obtained as:

$$\begin{aligned} F_{TA} &= 2k \cdot \Delta l_{TA} \\ &= 2k \cdot (\sqrt{r^2(1-\cos\alpha)^2 + (l + r\sin\alpha + h)^2} - l) \end{aligned} \ . \tag{3}$$

The vertical component F_{TAy} of the elastic force F_{TA} can be expressed as:

$$\begin{aligned} F_{TAy} &= F_{TA} \cdot \sin\beta_1 \\ &= F_{TA}\left(\frac{l + r\sin\alpha + h}{\sqrt{r^2(1-\cos\alpha)^2 + (l + r\sin\alpha + h)^2}}\right) \end{aligned} \ . \tag{4}$$

The moment M_{TA} generated by the elastic force F_{TA} about the torsional centre O can be obtained through the vector product of the vector $\overrightarrow{F_{TA}}$ and the vector $\overrightarrow{TO}$, as follows:

$$M_{TA} = \left|\overrightarrow{F_{TA}} \times \overrightarrow{TO}\right| = F_{TA} \cdot r \cdot \sin\theta_1 \ . \tag{5}$$

According to the geometric relationship in Fig. 2(b), it is known that $\theta_1 = \pi - (\beta_1 + \alpha)$, thus:

$$\begin{aligned} \sin\theta_1 &= \sin(\beta_1 + \alpha) \\ &= \sin\beta_1 \cos\alpha + \cos\beta_1 \sin\alpha \\ &= \frac{r\sin\alpha + (l+h)\cos\alpha}{\sqrt{r^2(1-\cos\alpha)^2 + (l + r\sin\alpha + h)^2}} \end{aligned} \ . \tag{6}$$

Substituting (6) into (5) yields:

$$M_{TA} = F_{TA} \frac{r^2\sin\alpha + r(l+h)\cos\alpha}{\sqrt{r^2(1-\cos\alpha)^2 + (l + r\sin\alpha + h)^2}} \ . \tag{7}$$

Similarly, the elastic forces of other springs and their moments about the torsional centre O can be derived using the same method, as follows:

For spring TC:

$$F_{TC} = 2k \cdot (\sqrt{r^2(1-\cos\alpha)^2 + (n - r\sin\alpha - h)^2} - n) \ , \tag{8}$$

$$F_{TCy} = F_{TC}\left(\frac{n - r\sin\alpha - h}{\sqrt{r^2(1-\cos\alpha)^2 + (n - r\sin\alpha - h)^2}}\right) , \tag{9}$$

$$\begin{aligned} M_{TC} &= \left|\overrightarrow{F_{TC}} \times \overrightarrow{TO}\right| = F_{TC} \cdot r \cdot \sin\theta_2 \\ &= F_{TC} \frac{-r^2\sin\alpha + r(n-h)\cos\alpha}{\sqrt{r^2(1-\cos\alpha)^2 + (n - r\sin\alpha - h)^2}} \end{aligned} \ , \tag{10}$$

For spring KB:

$$F_{KB} = 2k \cdot (\sqrt{r^2(1-\cos\alpha)^2 + (l - r\sin\alpha + h)^2} - l) \ , \tag{11}$$

$$F_{KBy} = F_{KB}\left(\frac{l - r\sin\alpha + h}{\sqrt{r^2(1-\cos\alpha)^2 + (l - r\sin\alpha + h)^2}}\right) \ , \tag{12}$$

$$\begin{aligned} M_{KB} &= \left|\overrightarrow{F_{KB}} \times \overrightarrow{KO}\right| = F_{KB} \cdot r \cdot \sin\theta_3 \\ &= F_{KB} \frac{-r^2\sin\alpha + r(l+h)\cos\alpha}{\sqrt{r^2(1-\cos\alpha)^2 + (l - r\sin\alpha + h)^2}} \end{aligned} \ , \tag{13}$$

For spring KD:

$$F_{KD} = 2k \cdot (\sqrt{r^2(1-\cos\alpha)^2 + (n + r\sin\alpha - h)^2} - n) \ , \tag{14}$$

$$F_{KDy} = F_{KD}\left(\frac{n + r\sin\alpha - h}{\sqrt{r^2(1-\cos\alpha)^2 + (n + r\sin\alpha - h)^2}}\right) \ , \tag{15}$$

$$\begin{aligned} M_{KD} &= \left|\overrightarrow{F_{KD}} \times \overrightarrow{KO}\right| = F_{KD} \cdot r \cdot \sin\theta_4 \\ &= F_{KD} \frac{r^2\sin\alpha + r(n-h)\cos\alpha}{\sqrt{r^2(1-\cos\alpha)^2 + (n + r\sin\alpha - h)^2}} \end{aligned} \ . \tag{16}$$

Thus, in this vibration amplitude state, the total vertical restoring force F_y and torsional moment M_α of the SSM are given by (17) and (18), respectively:

$$F_y = F_{TAy} - F_{TCy} + F_{KBy} - F_{KDy} \ , \tag{17}$$

$$M_\alpha = M_{TA} - M_{TC} - M_{KB} + M_{KD} \ . \tag{18}$$

The equivalent vertical stiffness K_h and torsional stiffness K_α of the SSM are derived by taking the partial derivatives of F_y with respect to vertical amplitude h, and M_α with respect to torsional angle α. Their expressions are as follows:

$$K_h = \frac{\partial F_y}{\partial h} = 8k - \Delta K_h \quad , \tag{19}$$

$$K_\alpha = \frac{\partial M_\alpha}{\partial \alpha} = 8kr^2 - \Delta K_\alpha \quad , \tag{20}$$

where:

$$\Delta K_h = 2k\left(\frac{l}{S_1} + \frac{n}{S_2} + \frac{l}{S_3} + \frac{n}{S_4} - \frac{p_1^2 l}{S_1^3} - \frac{p_2^2 n}{S_2^3} - \frac{p_3^2 l}{S_3^3} - \frac{p_4^2 n}{S_4^3}\right), \tag{21}$$

$$\begin{aligned}\Delta K_\alpha = 2k\Bigg(& 8r^2 \sin^2\frac{\alpha}{2} + \frac{q_1' l}{S_1} - \frac{q_2' n}{S_2} - \frac{q_3' l}{S_3} + \frac{q_4' n}{S_4} \\ & - \frac{q_1^2 l}{S_1^3} - \frac{q_2^2 n}{S_2^3} - \frac{q_3^2 l}{S_3^3} - \frac{q_4^2 n}{S_4^3}\Bigg)\end{aligned} . \tag{22}$$

S_1, S_2, S_3, and S_4 represent the deformed lengths of springs *TA*, *TC*, *KB*, and *KD*, respectively. Their expressions are given by:

$S_1 = \sqrt{r^2(1-\cos\alpha)^2 + (l + r\sin\alpha + h)^2}$;

$S_2 = \sqrt{r^2(1-\cos\alpha)^2 + (n - r\sin\alpha - h)^2}$;

$S_3 = \sqrt{r^2(1-\cos\alpha)^2 + (l - r\sin\alpha + h)^2}$;

$S_4 = \sqrt{r^2(1-\cos\alpha)^2 + (n + r\sin\alpha - h)^2}$;

p_1, p_2, p_3, and p_4 represent the vertical projections of the deformed lengths for springs *TA*, *TC*, *KB*, and *KD*, respectively. Their expressions are given by:

$p_1 = l + r\sin\alpha + h$;

$p_2 = n - r\sin\alpha - h$;

$p_3 = l - r\sin\alpha + h$;

$p_4 = n + r\sin\alpha - h$;

$q_1 = r^2\sin\alpha + r(l+h)\cos\alpha$;

$q_2 = -r^2\sin\alpha + r(n-h)\cos\alpha$;

$q_3 = -r^2\sin\alpha + r(l+h)\cos\alpha$;

$q_4 = r^2\sin\alpha + r(n-h)\cos\alpha$;

q_1', q_2', q_3', and q_4' represent the derivatives of the quantities q_1, q_2, q_3, and q_4 with respect to the torsional displacement α, respectively. Their expressions are given as follows:

$q_1' = r^2\cos\alpha - r(l+h)\sin\alpha$;

$q_2' = -r^2\cos\alpha - r(n-h)\sin\alpha$;

$q_3' = -r^2\cos\alpha - r(l+h)\sin\alpha$;

$q_4' = r^2\cos\alpha - r(n-h)\sin\alpha$;

When $\alpha = 0°$ and $h = 0$ m, the initial vertical stiffness K_{h0} and torsional stiffness $K_{\alpha0}$ of the SSM are determined as $8k$ and $8kr^2$, respectively.

III. Quantitative Case Analysis

A. Equivalent Vertical Stiffness and Torsional Stiffness

To quantitatively investigate the amplitude-dependent evolution of the equivalent vertical and torsional stiffnesses of the conventional SSM, the relevant parameters of the springs, segment model, and vibration amplitude ranges were specified, as listed in Table I. Based on the Table I parameters, the initial stiffness values were calculated as K_{h0} = 640 N/m and $K_{\alpha0}$ = 160 N·m/rad. Using (19) and (20), K_h and K_α under varying amplitude conditions were systematically computed. Surface plots depicting these stiffness-amplitude relationships were subsequently generated, as illustrated in Figs. 3 and 4.

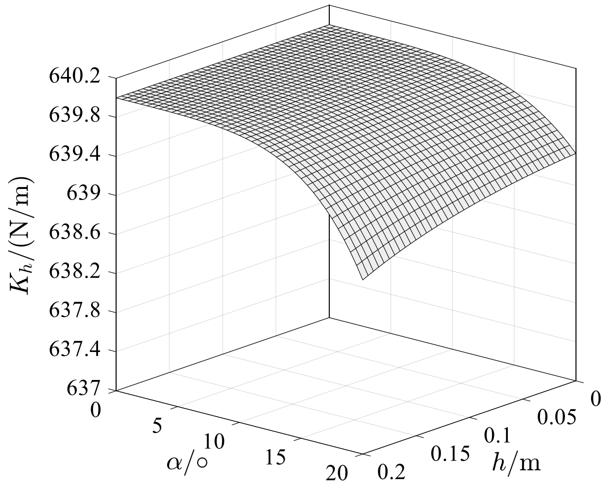

Fig. 3. Surface diagram of the equivalent vertical stiffness K_h.

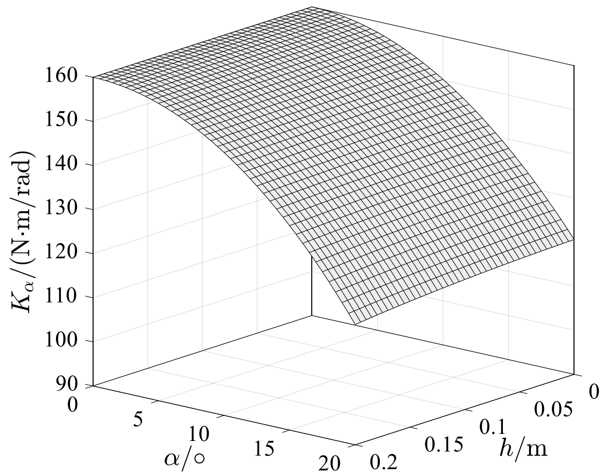

Fig. 4. Surface diagram of the equivalent torsional stiffness K_α.

Figs. 3 and 4 clearly show that both K_h and K_α decreased with increasing vibration amplitudes, but exhibited distinct reduction magnitudes; K_h underwent minimal reduction, while K_α showed significant degradation.

B. Reduction Rates of the Equivalent Vertical Stiffness and Torsional Stiffness

To quantitatively characterise the amplitude-dependent reduction trends in K_h and K_α, their respective reduction rates are defined as follows:

$$R_h = \frac{\Delta K_h}{8k} \times 100\% \quad , \tag{23}$$

$$R_\alpha = \frac{\Delta K_\alpha}{8kr^2} \times 100\% \quad , \tag{24}$$

where R_h and R_α denote the reduction rates of K_h and K_α, respectively; ΔK_h and ΔK_α were computed via (21) and (22).

K_h and K_α under varying amplitudes were calculated using (19) and (20), respectively, and visualised as 3D surface plots in Figs. 5 and 6. Fig. 5 shows that the maximum vertical stiffness reduction rate R_h remained < 0.19%, indicating a negligible influence of model vibration on the equivalent vertical stiffness. In contrast, Fig. 6 reveals a rapid increase in the torsional stiffness reduction rate R_α with increasing torsional amplitude. When the torsional amplitude α reached 20°, R_α reached approximately 25%, demonstrating that large-amplitude torsional vibrations significantly degrade the torsional stiffness of the system.

TABLE I
PARAMETERS FOR CALCULATING EQUIVALENT STIFFNESSES OF THE CONVENTIONAL SSM.

Parameter	Value
Single spring stiffness k	k = 80 N/m
Lateral distance r from the torsional centre to the spring attachment points (shown in Fig. 1)	r = 0.5 m
Initial lengths l and n of the upper and lower springs (shown in Fig. 1)	l = 1.2 m, n = 0.9 m
Mass M and the mass moment of inertia I_m of the segment model	M = 9.8 kg, I_m = 0.5 kg·m^2
Vertical amplitude range	0 m ≤ h ≤ 0.20 m
Torsional amplitude range	0° ≤ α ≤ 20°

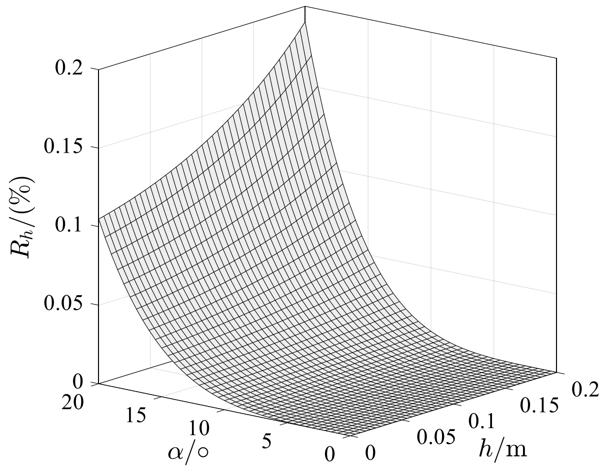

Fig. 5. Reduction rate R_h of the equivalent vertical stiffness K_h.

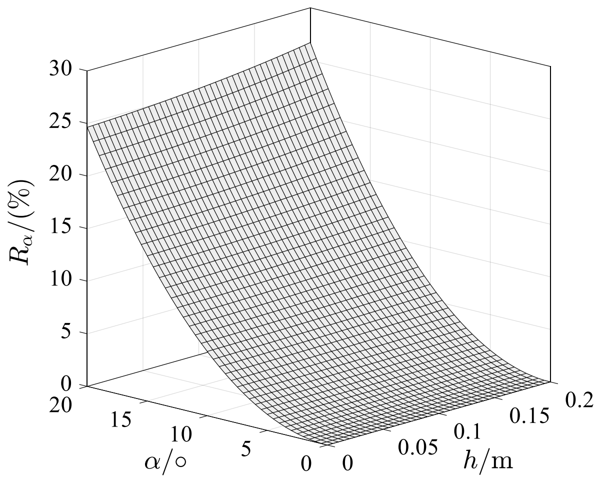

Fig. 6. Reduction rate R_α of the equivalent torsional stiffness K_α.

Fig. 7 presents the evolution of K_α versus the vertical amplitude h corresponding to the torsional amplitude α = 0°, 5°, 10°, 15°, and 20°. Notably, K_α remained constant when α = 0°, demonstrating that purely vertical vibrations do not affect the torsional stiffness. K_α decreased with increasing h, where the greater α is, the greater the reduction magnitude. Table II quantifies the reduction rates R_α (defined as the percentage decrease in K_α when h increased from 0 to 0.20 m) for different α. The maximum R_α observed was only 2.73%, confirming that K_α exhibited minimal sensitivity to vertical vibrations within the studied amplitude range.

Fig. 8 presents the evolution of K_α versus the torsional amplitude α corresponding to h = 0, 0.05, 0.10, 0.15, and 0.20 m. As shown, the K_α values for all six vertical amplitudes decreased rapidly with increasing torsional amplitude α, where higher vertical amplitudes exhibited more pronounced reduction magnitudes with α. Table III quantifies the reduction rates R_α (defined as the percentage decrease when α increased from 0° to 20°) for different h. The data demonstrate that R_α increased slightly with the vertical amplitude h, though the increment remained marginal. Compared with the h = 0 m case, the reduction rate R_α for h = 0.20 m showed an increase of only 2.05%, indicating that vertical vibration has a negligible influence on the equivalent torsional stiffness of the SSM.

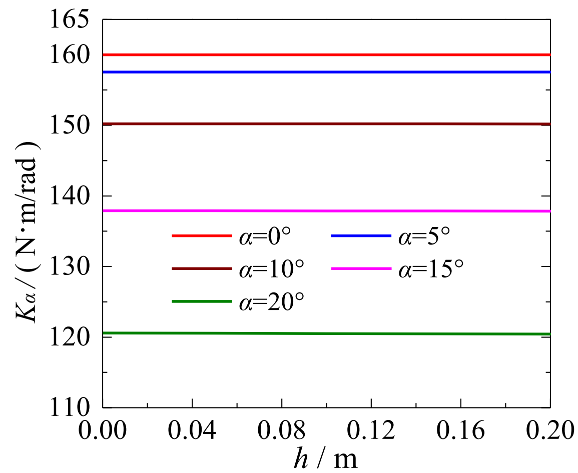

Fig. 7. Evolution curves of K_α corresponding to different torsional amplitudes versus the vertical amplitude h.

TABLE II
REDUCTION RATES OF THE EQUIVALENT TORSIONAL STIFFNESS CORRESPONDING TO DIFFERENT TORSIONAL AMPLITUDES.

α / °	0	5	10	15	20
R_α / %	0	0.09	0.40	1.12	2.73

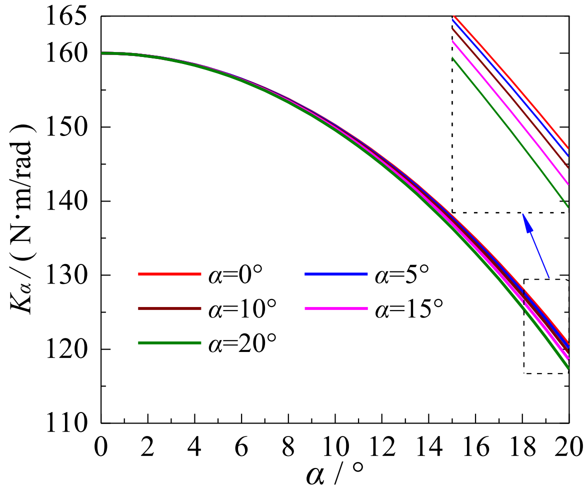

Fig. 8. Evolution curves of K_α corresponding to different vertical amplitudes versus the torsional amplitude α.

TABLE III
REDUCTION RATES OF THE EQUIVALENT TORSIONAL STIFFNESS CORRESPONDING TO DIFFERENT VERTICAL AMPLITUDES.

h / m	0	5	10	15	20
R_α / %	24.64	24.91	25.32	25.90	26.69

Based on the above quantitative analysis, within the investigated amplitude ranges (0 m ≤ h ≤ 0.20 m, 0° ≤ α ≤ 20°), the vertical vibration exerted negligible influence on both the equivalent vertical stiffness K_h and equivalent torsional stiffness K_α of the conventional SSM. Therefore, to simplify the analysis, the effects of the model vibration on K_h and vertical vibration on K_α were neglected. The simplified formulae for K_h and K_α of the conventional SSM are as follows:

$$K_h = K_{h0} = 8k \quad , \tag{25}$$

$$K_\alpha = \frac{\partial M_\alpha}{\partial \alpha} = 8kr^2 - \Delta K_\alpha \quad , \tag{26}$$

where ΔK_α is still defined by (22) but differs in that the effects of vertical motion are neglected in (26). The denotations of the symbols in the ΔK_α expression are as follows:

$S_1 = \sqrt{r^2(1-\cos\alpha)^2 + (l + r\sin\alpha)^2}$;

$S_2 = \sqrt{r^2(1-\cos\alpha)^2 + (n - r\sin\alpha)^2}$;

$S_3 = \sqrt{r^2(1-\cos\alpha)^2 + (l - r\sin\alpha)^2}$;

$S_4 = \sqrt{r^2(1-\cos\alpha)^2 + (n + r\sin\alpha)^2}$;

$p_1 = l + r\sin\alpha$;

$p_2 = n - r\sin\alpha$;

$p_3 = l - r\sin\alpha$;

$p_4 = n + r\sin\alpha$;

$q_1 = r^2\sin\alpha + rl\cos\alpha$;

$q_2 = -r^2\sin\alpha + rn\cos\alpha$;

$q_3 = -r^2\sin\alpha + rl\cos\alpha$;

$q_4 = r^2\sin\alpha + rn\cos\alpha$;

$q_1' = r^2\cos\alpha - rl\sin\alpha$;

$q_2' = -r^2\cos\alpha - rn\sin\alpha$;

$q_3' = -r^2\cos\alpha - rl\sin\alpha$;

$q_4' = r^2\cos\alpha - rn\sin\alpha$;

C. Vibration Frequencies and the Reduction Rates of Torsional Frequency

Notably, (26) maintains the same form as (20), but explicitly neglects the influence of vertical vibration on K_α by retaining only the torsional vibration effect. This simplification enhances the computational efficiency while preserving engineering practicality.

Neglecting the coupling effect between vertical vibration and torsional vibration, the vertical vibration frequency f_h and torsional vibration frequency f_α of the conventional SSM can be determined based on K_h, K_α, the segment model mass M, and mass moment of inertia I_m, as follows:

$$f_h = \frac{1}{2\pi}\sqrt{\frac{K_h}{M}} = \frac{1}{2\pi}\sqrt{\frac{8k}{M}} \quad ; \tag{27}$$

$$f_\alpha = \frac{1}{2\pi}\sqrt{\frac{8kr^2 - \Delta K_\alpha}{I_m}} \quad . \tag{28}$$

As the influence of the model vibration on K_h is neglected, the vertical vibration frequency f_h remains constant. Using (27) and the given parameters, f_h was calculated to be 1.286 Hz. The torsional vibration frequency f_α depends on the torsional amplitude α, where the initial torsional frequency $f_{\alpha 0}$ (i.e., the frequency at α = 0°) was 2.847 Hz. Fig. 9 illustrates the variation in f_α with the torsional amplitude α, revealing that f_α decreased as α increased, with the rate of decrease accelerating at higher amplitudes.

To quantify the reduction in the torsional frequency, the reduction rate Rf_α is defined as:

$$Rf_\alpha = 1 - \sqrt{1 - R_\alpha} \quad , \tag{29}$$

where Rf_α is governed by the reduction rate R_α, and R_α is calculated via (24). The evolution of Rf_α with α, plotted in Fig. 9, demonstrates that Rf_α increased progressively with α, exhibiting an accelerating growth rate. When $\alpha \le 5°$, $Rf_\alpha < 1\%$, indicating negligible torsional frequency variation in practical segment model experiments. For $\alpha > 5°$, Rf_α increased rapidly, reaching a torsional frequency reduction rate of 13.19% at α = 20°. Consequently, in terms of geometric nonlinearity, it is recommended that the maximum torsional amplitude of conventional spring suspension systems should not exceed 5°. However, it should be emphasised that the actual maximum allowable α is also influenced by mass nonlinearity, damping nonlinearity of the system, and lateral vibrations of the springs.

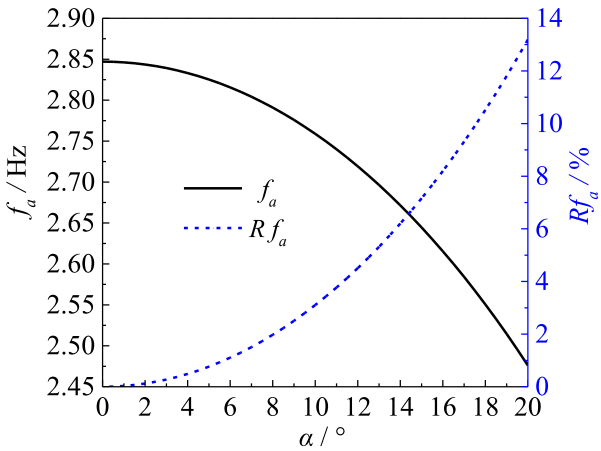

Fig. 9 Evolution curves of f_α and Rf_α versus the torsional amplitude α.

IV. Conclusion

This study investigated the nonlinear stiffness characteristics of conventional SSMs typically employed for assessing the wind-resistant performance of bridges. Using a 2D mechanical model, analytical expressions for the equivalent vertical K_h and torsional K_α stiffness were derived. A numerical case study quantified the effects of vertical and torsional amplitudes on equivalent stiffness and vibration frequency. The main findings are summarised as follows:

(1) Vertical and torsional vibrations exhibited negligible influence on K_h. Within the amplitude ranges (0 m ≤ h ≤ 0.20 m; 0° ≤ α ≤ 20°), the reduction rate R_h remained < 0.19%.

(2) The equivalent torsional stiffness K_α of the suspension system is significantly affected by the torsional vibrations of the model, which displayed a notable amplitude-dependent nonlinearity. As the torsional amplitude α increased, K_α decreased significantly. When a vertical vibration was absent (h = 0 m), the reduction rates R_α of K_α were 6.11% and 24.64% for torsional amplitudes of 10° and 20°, respectively. When α = 20° and the vertical amplitude h increased from 0 to 0.20 m, the decrease in K_α increased slightly from 24.64% to 26.69%. This indicates that the vertical vibration of the

model has a minimal impact on the torsional stiffness of the system.

(3) The vertical frequency f_h of the SSM showed limited sensitivity to both vertical and torsional vibrations. Additionally, vertical vibrations had no effect on the torsional frequency f_α. In contrast, torsional vibrations exhibited significant amplitude-dependent nonlinearity; as the torsional vibration amplitude increased, f_α experienced a notable nonlinear reduction. In the case study presented, when the angle $\alpha \leq 5°$, the reduction rate Rf_α remained < 1%. Therefore, to minimise geometric nonlinearity, it is recommended that the torsional amplitude in conventional spring suspension devices be limited to 5°. When $\alpha > 5°$, Rf_α increased significantly; for example, at $\alpha = 20°$, the frequency decreased by 13.19%. Therefore, nonlinear torsional stiffness must be explicitly considered when identifying aerodynamic derivatives or assessing wind-resistant performance of bridge sections under large-amplitude conditions using the conventional SSMs.

The derived formulae for the equivalent stiffnesses (K_h and K_α) of the conventional SSM are universally applicable. However, the conclusions, such as the numerical values or trends, obtained through the quantitative analysis of specific examples may not necessarily be applicable to other SSMs with other parameter settings, and specific analyses should be conducted considering the actual circumstances. Moreover, in subsequent research, rigorous wind tunnel tests on the SSM must be designed and conducted to further validate the theoretical findings presented in this study.

REFERENCES

[1] Lei Yan, Le-Dong Zhu, Xu-Hui He, and Richard G.J. Flay, “Experimental determination of aerodynamic admittance functions of a bridge deck considering oscillation effect,” Journal of Wind Engineering and Industrial Aerodynamics, vol. 190, pp83-97, 2019.

[2] Bo Wu, Huo-Ming Shen, Hai-Li Liao, Qi Wang, and Liu Jun, “Identification of amplitude-dependent damping ratio and flutter derivatives of a streamlined box girder under various wind angles of attack,” Journal of Bridge Engineering, vol. 28, no. 7, pp04023041, 2023.

[3] Yun-Fei Wang, Xin-Zhong Chen, and Yong-Le Li, “Nonlinear self-excited forces and aerodynamic damping associated with vortex-induced vibration and flutter of long span bridges,” Journal of Wind Engineering and Industrial Aerodynamics, vol. 204, pp104207, 2020.

[4] Lin Zhao, Feng-Ying Wu, Ting-Shu Han, Ling-Yao Li, Tao Pan, Hai-Zhu Xiao, and Yao-Jun Ge, “Aerodynamic force distribution and vortex drifting pattern around a double-slotted box girder under vertical vortex-induced vibration,” Journal of Wind Engineering and Industrial Aerodynamics, vol. 241, pp105548, 2023.

[5] Zheng-Qing Chen, Xiao Xiao, Zhi-Wen Huang, and Xu-Gang Hua, “Influence of the nonlinearity of spring-suspended sectional model systems on Identification of vortex-induced vibration parameters,” Journal of Railway Science and Engineering, 2021, 18(4): 821-829. (In Chinese)

[6] Gianni Bartoli, Stefano Contri, Claudio Mannini, and Michele Righi, “Toward an improvement in the identification of bridge deck flutter derivatives,” Journal of Engineering Mechanics, vol. 135, no. 8, pp771-785, 2009.

[7] Fu-You Xu, Xu-Yong Ying, Yong-Ning Li, and Ming-Jie Zhang, “Experimental explorations of the torsional vortex-induced vibrations of a bridge deck,” Journal of Bridge Engineering, vol. 21, no. 12, pp04016093, 2016.

[8] Fu-You Xu, and Zhan-Biao Zhang, “Free vibration numerical simulation technique for extracting flutter derivatives of bridge decks,” Journal of Wind Engineering and Industrial Aerodynamics, vol. 170, pp226-237, 2017.

[9] Sébastien Maheux, J. Peter C. King, Ashraf El Damatty, and Fabio Brancaleoni, “Theory for nonlinear section model tests in the wind tunnel for cable-supported bridges,” Engineering Structures, vol. 266, pp114623, 2022.

[10] Luca Pigolotti, Claudio Mannini, Gianni Bartoli, and Klaus Thiele, “Critical and post-critical behaviour of two-degree-of-freedom flutter-based generators.” Journal of Sound and Vibration, vol. 404, pp116-140, 2017.

[11] Guang-Zhong GAO, Le-Dong Zhu, Wan-Shui Han, and Jia-Wu Li, “Nonlinear post-flutter behavior and self-excited force model of a twin-side-girder bridge deck,” Journal of Wind Engineering and Industrial Aerodynamics, vol. 177, pp227-241, 2018.

[12] Guang-Zhong Gao, Le-Dong Zhu, Jia-Wu Li, Wan-Shui Han, Li-Bo Wei, and Qing-Chen Yan, “Nonlinear post-flutter bifurcation of a typical twin-box bridge deck: Experiment and empirical modeling,” Journal of Fluids and Structures, vol. 112, pp103583, 2022.

[13] Kai Li, Yan Han, C. S. Cai, and Zhi-Xiong Qiu, “A general modeling framework for large-amplitude 2DOF coupled nonlinear bridge flutter based on free vibration wind tunnel tests,” Mechanical Systems and Signal Processing, pp222, pp111756, 2025.

[14] Yan Han, Jun Song, Kai Li, and Peng Hu, “Wind tunnel tests study on nonlinear characteristics of structural and aerodynamic damping of steel truss girder section under large-amplitude post-flutter,” China Journal of Highway and Transport, vol. 36, no. 7, pp56-66, 2023. (In Chinese)

[15] Ming-Jie Zhang, Fu-You Xu, and Xu-Yong Ying, “Experimental investigations on the nonlinear torsional flutter of a bridge deck,” Journal of Bridge Engineering, vol. 22, no.8, pp04017048, 2017.

[16] Chuan-Xin Hu, Lin Zhao, and Gao-Jun Ge, “Wind-Induced instability mechanism of old Tacoma narrows bridge from aerodynamic work perspective,” Journal of Bridge Engineering, vol. 27, no.5, pp04022029, 2022.

[17] Bo Wu, Xin-Zhong Chen, Qi Wang, Hai-Li Liao, and Jia-Hui Dong, “Characterization of vibration amplitude of nonlinear bridge flutter from section model test to full bridge estimation,” Journal of Wind Engineering and Industrial Aerodynamics, vol. 197, pp104048, 2020.

[18] Zhi-Tian Zhang, Zhi-Xiong Wang, Kai Qie, and Bu-Hao Tan, “Influences of the torsional-bending frequency ratio on post-flutter characteristics of a π-shaped section model,” Journal of Vibration Engineering, vol. 34, no. 6, pp1268-1275, 2021. (In Chinese)

[19] Rui-Lin Zhang, Hong-Bo Yang, Zhi-Wen Liu, Jian Yang, and Zheng-qing Chen, “Segmental model tests for post flutter characteristics of truss-stiffening girder suspension bridge,” Journal of Vibration and Shock, vol. 41, no. 5, pp1-8+19, 2022. (In Chinese)

[20] Guang-Zhong Gao, and Le-Dong Zhu, “Nonlinearity of mechanical damping and stiffness of a spring-suspended sectional model system for wind tunnel tests,” Journal of Sound and Vibration, vol. 355, pp369-391, 2015.

[21] Y. Tang, X. G. Hua, Z. Q. Chen, and Y. Zhou, “Experimental investigation of flutter characteristics of shallow Π section at post-critical regime[J]. Journal of Fluids and Structures, vol. 88, pp275-291, 2019.

[22] Zhi-Tian Zhang, Zhi-Xiong Wang, Jia-Dong Zeng, Le-Dong Zhu, and Yao-Jun Ge, “Experimental investigation of post-flutter properties of a suspension bridge with a π-shaped deck section,” Journal of Fluids and Structures, vol. 112, pp103592, 2022.

[23] Ming-Jie Zhang, and Fu-You Xu, “Nonlinear vibration characteristics of bridge deck section models in still air,” Journal of Bridge Engineering, vol. 23, no. 9, pp04018059, 2018.

[24] Fu-You Xu, and Zhan-Biao Zhang, “Numerical simulation of windless-air-induced added mass and damping of vibrating bridge decks,” Journal of Wind Engineering and Industrial Aerodynamics, vol. 180, pp98-107, 2018.

[25] Zhan-Biao Zhang, and Fu-You Xu, “Added mass and damping effects on vibrating bridge decks in still air,” Journal of Wind Engineering and Industrial Aerodynamics, vol. 191, pp227-238, 2019.

[26] Fu-You Xu, Pin-Qing Wang, and Jing Yang, “Geometric nonlinear stiffness and frequency of the conventional spring-suspended free-vibration testing device,” Journal of Wind Engineering and Industrial Aerodynamics, vol. 242, pp105585, 2023.

Dr. Changqing Wu was born in October 1987 and received his Ph.D. Degree from Hunan University, Changsha, China, in 2019. He is a lecturer at the College of Civil Engineering and Architecture, Hunan Institute of Science and Technology, Yueyang, China. His research interests cover bridge wind resistance and structural vibration control. He has published more than 20 technical papers.